



Deposited via The University of Sheffield.

White Rose Research Online URL for this paper:

<https://eprints.whiterose.ac.uk/id/eprint/131637/>

Version: Accepted Version

Article:

Kumar, A., Pillai, P.B., Song, X. et al. (2018) Negative Capacitance beyond Ferroelectric Switches. ACS Applied Materials and Interfaces, 10 (23). pp. 19812-19819. ISSN: 1944-8244

<https://doi.org/10.1021/acsami.8b05093>

This document is the Accepted Manuscript version of a Published Work that appeared in final form in ACS Applied Materials and Interfaces, copyright © American Chemical Society after peer review and technical editing by the publisher. To access the final edited and published work see <https://doi.org/10.1021/acsami.8b05093>.

Reuse

Items deposited in White Rose Research Online are protected by copyright, with all rights reserved unless indicated otherwise. They may be downloaded and/or printed for private study, or other acts as permitted by national copyright laws. The publisher or other rights holders may allow further reproduction and re-use of the full text version. This is indicated by the licence information on the White Rose Research Online record for the item.

Takedown

If you consider content in White Rose Research Online to be in breach of UK law, please notify us by emailing eprints@whiterose.ac.uk including the URL of the record and the reason for the withdrawal request.

Negative Capacitance beyond ferroelectric switches

*Ashwani Kumar, Premlal Balakrishna Pillai, Xiaoyao Song, and Maria Merlyne De Souza**

Department of Electronic and Electrical Engineering, University of Sheffield–North Campus, S3
7HQ Sheffield, United Kingdom

KEYWORDS: Negative Capacitance, subthreshold slope, solid electrolyte, ferroelectric, field effect transistors, Tantalum oxide, zinc oxide.

ABSTRACT: Negative capacitance transistors are a unique class of switches capable of operation beyond the Boltzmann limit to realise sub-thermionic switching. Until now, the negative capacitance effect has been predominantly attributed to devices employing an unstable insulator with ferroelectric properties, exhibiting a two-well energy landscape, in accordance with Landau theory. The theory and operation of a solid electrolyte Field Effect Transistor (SE-FET) of subthreshold swing less than 60 mV/dec in the absence of a ferroelectric gate dielectric is demonstrated in this work. Unlike ferroelectric FETs that rely on a sudden switching of dipoles to achieve negative capacitance, we demonstrate a distinctive mechanism that relies on the accumulation and dispersion of ions at the interfaces of the oxide, leading to a subthreshold slope (SS) as low as 26 mV/dec in these samples. The frequency of operation of these unscaled devices lies in a few milli-Hertz, because at higher or lower frequencies, the ions in the insulator are either too fast or too slow to produce voltage amplification. This is unlike Landau switches, where the

SS remains below $60\text{mV}/\text{dec}$ even under quasi-static sweep of the gate bias. The proposed FETs show a higher on-current with thicker oxide in the entire range of gate voltage, clearly distinguishing their scaling laws from those of ferroelectric FETs. Our theory validated with experiment, demonstrates a new class of devices capable of negative capacitance that opens up alternate methods of steep switching beyond the traditional approach of Ferroelectric or memristive FETs.

INTRODUCTION

Complementary Metal Oxide Semiconductor (CMOS) technology is the main driver of the contemporary information age. Its pervasiveness has been delivered by an exponential increase in processing power of a chip via a continuous reduction in the physical dimensions of transistors by almost a factor of half, every 18 months, according to Moore's law. Despite continuous downscaling, a proportional reduction in the supply voltage has been a greater challenge since the last decade, resulting in higher density chips with increased power consumption today. This limitation arises because the drain to source current, I_{DS} , that is proportional to the gate induced carrier density N , is exponentially dependent on the semiconductor surface potential (Ψ_s)¹, i.e., $I_{DS} \propto N \propto \exp(q\Psi_s/k_B T)$, requiring Ψ_s to change by at least $\sim 60\text{ mV}$ for an order of magnitude (a decade) change in I_{DS} . Overcoming this Boltzmann limit of $2.3 k_B T/q \approx 60\text{ mV}/\text{dec}$ (where k_B is the Boltzmann constant, T , the temperature and q the elementary charge) of the sub-threshold swing (SS) of a Metal–Oxide–Semiconductor Field Effect Transistor (MOSFET) is considered as a possible evolution of CMOS scaling below a channel length of 8 nm for future logic devices²⁻⁴. Broadly speaking, beyond the relationship between Ψ_s and I_{DS} as indicated above, the SS is affected by how well the gate can be coupled to the semiconductor, via the body factor m , where

V_{GS} is the applied potential at the gate, distributed across the gate dielectric and the semiconductor region of a typical transistor as

$$V_{GS} = \phi_{ms} + V_{ox} + \Psi_s \quad (1)$$

Where ϕ_{ms} represents the difference in work function between the gate and semiconductor, and V_{ox} is the potential drop across the dielectric. In such a case, for a constant ϕ_{ms} , m , the body factor can be expressed as $m = dV_{GS}/d\Psi_s$. If the capacitances associated with the gate dielectric and the semiconductor are represented as C_{ins} and C_{sc} respectively, the body factor m is equal to $1 + C_{sc}/C_{ins} > 1$, giving rise to a subthreshold swing², $SS = m \times 2.3k_B T/q = m \times n > 60 \text{ mV/dec}$ in conventional transistors. A change in the surface potential ($d\Psi_s$) larger than the change in the applied gate bias (dV_{GS}) is required to achieve $m < 1$.

A number of alternative approaches, broadly considered subsets of “Steep Subthreshold devices”, are now being contemplated to achieved $m < 1$. Techniques that result in $m < 1$, also largely referred to as Landau switches⁵, are of great significance to technology, as they result in low operating voltages and thereby reduced power consumption of electronic circuits. Amongst such techniques, reported to date, the most promising for future technology nodes are ferroelectric FETs (FE-FETs)^{6,7}, initiated by the pioneering work of Salahuddin and Datta in 2008⁸, though others, such as piezoelectric FETs^{9,10}, nanoelectro-mechanical FETs (NEMFETs)¹¹⁻¹³, and phase-FETs^{14,15}, employing a resistive switch have also been reported. There are two important distinctions in approach amongst the various mechanisms that are described. In one case, the net capacitance between the gate and the semiconductor channel is boosted by introducing a material in the gate dielectric stack with an inherent instability, such as in a FE-FETs or a NEMFET⁵, depicted in Figure 1 (a). In these FETs, the energy profile of the gate dielectric stack exhibits a dual energy-well that upon transition from one well to the other, leads to a negative capacitance

$C_{FE/NEM}$. In the second case, the abrupt switching of a resistive switch in series with the current flow path, between a low resistance state (LRS) and a high resistance state (HRS), is utilised to produce steep switching. The resistive switch is typically realised either with a material exhibiting insulator-to-metal transition (IMT) such as vanadium dioxide¹⁴ or a memristor element, as in Figure 1 (b), realised either via a phase change memory (PCM), electrochemical metallization memory (ECM), or valence change memory (VCM)¹⁶. In PCMs, a change in the phase of a material, e.g. GeTe or Sb₂Te₃, from the amorphous to crystalline or vice-versa ‘sets’ or ‘resets’ the device in the LRS or HRS. The ECM consists of an active electrode of Ag or Cu and a counter electrode of e.g. Pt separated by an insulating layer of solid electrolyte, e.g. SiO₂ or Ta₂O₅, where resistive switching from the HRS to the LRS takes place via migration of metallic ions from the active electrodes into the insulator, thus forming a conducting filament.¹⁷ In the case of a VCM, the movement of negatively charged oxygen ions or positively charged vacancies in the thin film (~10 nm) of, for example TaOx, HfOx, or TiOx, results in the formation/dissolution of a vacancy rich conducting filament that is responsible for resistive switching.¹⁸

In this work, we demonstrate an alternate Negative Capacitance mechanism to achieve steep switching characteristics but only under dynamic operation in Ta₂O₅/ZnO solid electrolyte (SE-) FETs, shown in Figure 1 (c). As indicated in this figure, the presence of doubly charged mobile oxygen ions and vacancies in the Ta₂O₅, induces a sheet charge at the interface of Ta₂O₅ and ZnO, which gives rise to an additional electrolytic capacitance, indicated by C_{EL} in the equivalent circuit diagram. We develop a theoretical framework that provides evidence that under a dynamic sweep of the gate bias, C_{EL} achieves a negative value such that $|C_{EL}| > C_{ins}$, leading to sub-60 mV/dec switching, yet without the involvement of any ferroelectric material or filamentary processes in the gate insulator.

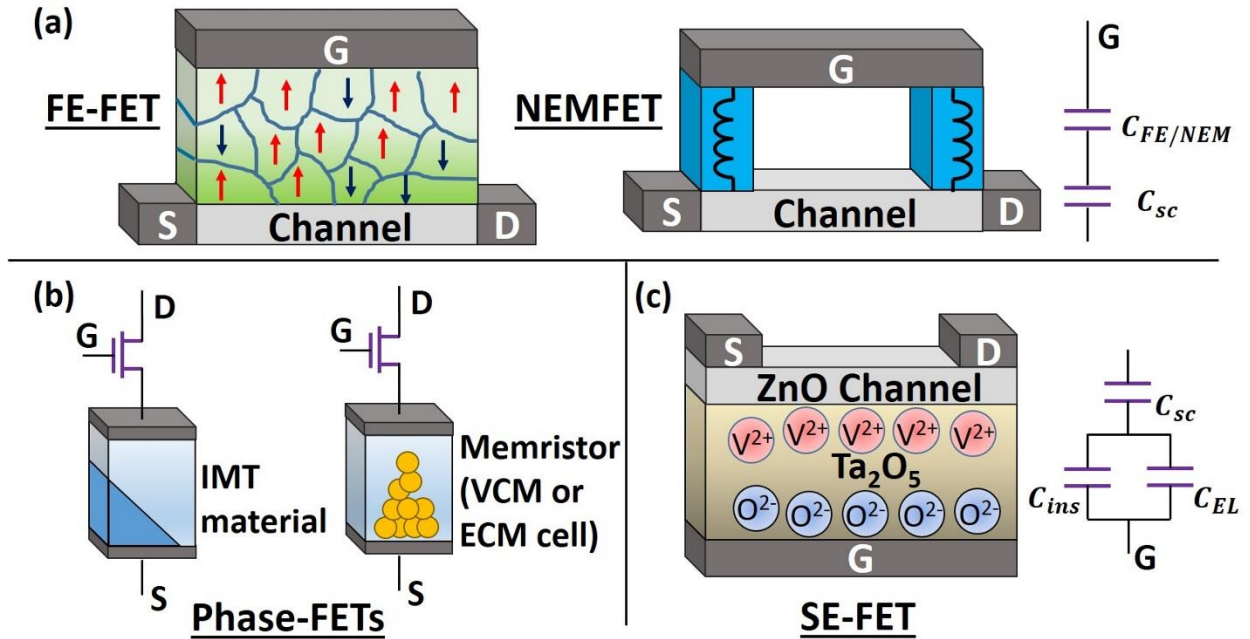


Figure 1. Various schemes for sub-60 mV/dec switching. (a) Device schematic of a FE-FET (LHS) and a NEMFET (RHS) where due to either the switching of domains in the FE-FET, or electromechanical motion of the gate in the NEMFET, $C_{FE/NEM}$ becomes negative, resulting in a body factor $m = 1 + C_{sc}/C_{FE/NEM} < 1$ and $SS < 60 \text{ mV/dec}$. (b) Phase-FETs, where a resistive switch either consisting of a material exhibiting insulator-to-metal phase transition (IMT) (LHS) or a memristor (VCM or ECM) (RHS) is included in the current path of an ordinary FET. (c) Schematic of a Ta_2O_5/ZnO device and the equivalent gate circuit model of the MOS capacitor, indicating charge separation of oxygen ions and vacancies at respective opposite interfaces of the Ta_2O_5 . An additional capacitance C_{EL} arises as a result, in parallel with the gate dielectric capacitor C_{ins} .

EXPERIMENTAL METHODS

Our alternate mechanism for steep switching is demonstrated in bottom gated three-terminal thin-film transistors, as shown in Figure 1 (c). A conducting Indium Tin Oxide (ITO, $20 \Omega/\text{square}$)

is used as gate, thicknesses of 120 and 275 nm of tantalum oxide (Ta_2O_5) of dielectric constant $\epsilon_{Ta_2O_5} \approx 20.8$ are deposited as the gate insulator and 40 nm of zinc oxide as channel, via RF sputtering as reported in ref ¹⁹. The sputtered Ta_2O_5 results in an amorphous phase, as the temperature required for crystallisation is more than 1000 K²⁰. All the measurements of electrical characteristics are carried out using an Agilent B1500.

RESULTS AND DISCUSSION

The drain current characteristics are examined in the forward and backward directions at scan rates of gate voltage ranging from 2.17 mHz to 15.65 mHz in Figure 2 (a). During the backward sweep, a two-fold reduction in the average subthreshold swing is observed when the scan rate is reduced from 15.65 mHz to 2.17 mHz, while the gate leakage current of the device always remains below 1 nA, as displayed in the inset. Unlike the conventional clockwise hysteresis associated with charge trapping at oxide/semiconductor interfaces that leads to a reduction in the drain current during the backward sweep,²¹ the anticlockwise hysteresis in the transfer characteristics, as well as its dependence on the scan rate, indicates the presence of an electric field dependent memory effect arising from ionic motion in the insulator that closely resembles the flipping of electric dipoles in a ferroelectric FET.²² In the present case, factors governing the value of m can be understood from the relationship of the surface potential of the channel in response to an applied gate voltage, which in its simplest form is given as

$$V_{GS} = \phi_{ms} + \frac{Q_{ch}}{C_{ins}} - \frac{Q_{ox}}{C_{ins}} + \Psi_s \quad (2)$$

C_{ins} is the unit area capacitance of the gate insulator, Q_{ox} is the sheet charge density at the interface of the oxide and semiconductor, and Q_{ch} is the sheet charge density in the semiconductor. In the present case, due to accumulation-dispersion of ions and vacancies within the gate dielectric

under dynamic sweep of the gate voltage, the charge in the insulator, Q_{ox} varies with the applied gate bias. Under such conditions, the body factor is described by an alternate expression of device capacitances as

$$m = 1 + \frac{C_{sc}}{C_{EL} + C_{ins}} \quad (3)$$

Where C_{EL} is defined as dQ_{ox}/dV_{ox} . Details of the derivation of Equation (3) are described in Supplementary Note 1. In the present case, if the rate of change of vacancies dQ_{ox}/dt at the interface of Ta_2O_5 with the semiconductor is higher than the rate of change of bias across the oxide V_{ox}/dt , the resulting C_{EL} turns negative with a magnitude greater than C_{ins} , resulting in m less than unity according to Eq. (3). Electrolyte gated transistors have been used in the past to achieve high carrier densities²³, realise non-volatile memories²⁴, reduce operating voltage²⁵, or reduce subthreshold slope but only down to $82 \text{ mV}/dec$ ²⁶ to our knowledge.

Whilst negative capacitance under dynamic conditions has been observed in materials ranging from crystalline to amorphous inorganic semiconductors and organic compounds^{27,28}, it has previously been attributed to minority carrier flow, interface states, slow transient time of the carriers, or space charge²⁸. This is the first instance of dynamic negative capacitance at a suitable scan rate to obtain a $SS < 60 \text{ mV}/dec$ in thin film transistors. As the gate sweep frequency is increased beyond $\sim 20 \text{ mHz}$, a sub- $60 \text{ mV}/dec$ of SS disappears as shown in Figure 2 (b), as the phenomenon requires ionic motion within the insulator to equilibrate with the applied gate electric field.

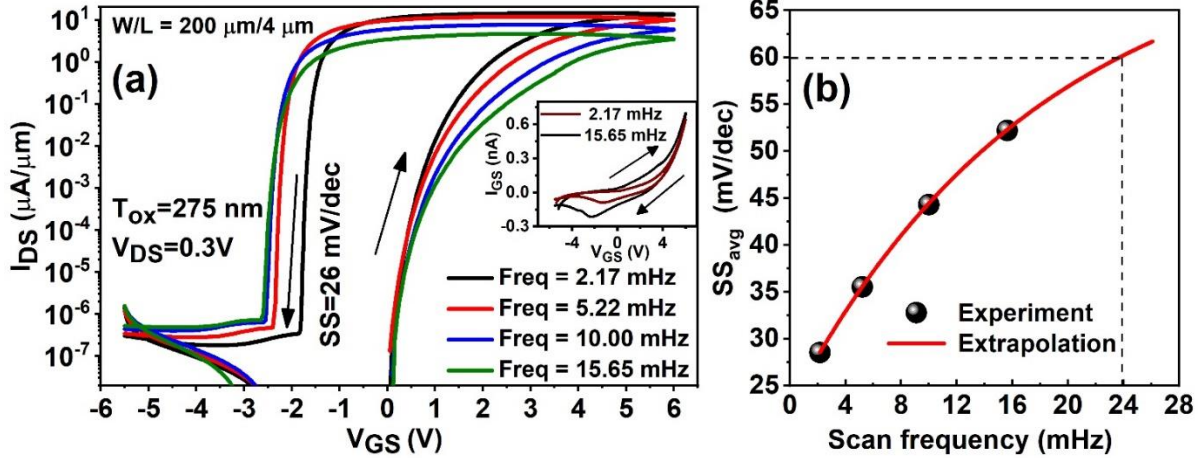


Figure 2. Measured Transfer characteristics and subthreshold swing. (a) Dependence of the switching properties of fabricated ZnO/Ta_2O_5 SE-FETs on the scan rate of the gate voltage and the corresponding gate current characteristics. Transfer characteristics are captured under forward and reverse sweeps for frequencies ranging from 2.17 mHz to 15.65 mHz, corresponding to scan rates of 0.05 V/s – 0.36 V/s. A step subthreshold swing of 26 mV/dec is obtained corresponding to the lowest sweep frequency. (b) Dependence of the subthreshold swing extracted from the $I_{DS} - V_{GS}$ characteristics in (a) in the reverse sweep, on the scan frequency. The subthreshold slope begins to exceed 60 mV/dec beyond 23 mHz of the gate sweep in the reverse direction.

Our model is based upon the drift and diffusion of doubly charged negative oxygen ions²⁹ in the Ta_2O_5 solid electrolyte (SE) under an electric field, as described by the point ion model of Mott and Gurney^{30,31}, more details of which are presented in Supplementary Note 2. The parameters used in the model are described in Supplementary Tables S1 and S2. Ta_2O_5 amongst other oxides such as HfO_2 and TiO_x , is widely known to contain oxygen ions and vacancies whose dynamics have been utilised to explain the resistive switching behaviour in valence change memory (VCM) cells. Some metal cations such as W , Ta , Ti , and Hf can participate in the oxygen exchange

reactions by diffusing from the metal contact into the insulator in the vicinity of the interface, which can affect the electrical properties of thin films ($\sim 7\text{ nm}$) of Ta_2O_5 .³² On the other hand, Indium Tin Oxide (ITO), employed as a bottom gate, is known for its electrical and chemical stability and has been used for preventing the diffusion of specific metallic ions.³³ While there is some evidence of diffusion of Indium ions inside an organic material after a long-term operation in Organic LEDs³⁴ and in some polymers,³⁵ to the best of our knowledge no evidence is available for the diffusion of such ions from Indium Tin Oxide (ITO) or ZnO into other oxides. We, therefore, neglect the role of other mobile species in our analysis.

Figure 3 (a) shows a comparison of the measured and simulated transfer characteristics during the forward and backward gate sweeps at a scan frequency of 10 mHz for a Ta_2O_5 thickness of 275 nm , with a SS of 35 mV/dec . This thickness and scan rate are selected due to a wider hysteresis that makes it easy to visualise regions of internal voltage amplification ($a \rightarrow b$ and $c \rightarrow d$) in the figures. During the forward sweep, the doubly charged oxygen ions are driven towards the gate/ Ta_2O_5 while the positively charged vacancies are accumulated at the Ta_2O_5/ZnO interface, resulting in a build-up of positive interface charge density Q_{ox} at this interface, as shown in Figure 3 (b). During the backward scan of the gate bias, as V_{GS} is reduced from its maximum point, Q_{ox} continues to rise to its maximum value at a gate bias of $\sim 2.5\text{ V}$, highlighted by the dashed circle in Figure 3 (b), well below the maximum applied voltage of 6 V . This is attributed to the delay in achieving its steady state value, owing to the poor mobility of oxygen ions, estimated as $1.12 \times 10^{-11}\text{ cm}^2/\text{Vs}$ via Chronoamperometry measurements of the gate current²¹ described using the Cottrell equation³⁶ (See Supplementary Table S2 for a summary of model parameters). This build-up of Q_{ox} also helps to maintain the sheet charge density Q_{ch} in the semiconductor channel, and therefore a higher drain current in the reverse sweep. Until point a ,

the surface potential of the channel is maintained by Q_{ch} , while the entire drop in gate potential occurs across Ta_2O_5 . Beyond point a , as V_{GS} reduces further, a sudden depletion in Q_{ox} (see inset Figure 3 (b)), causes the drain current to drop sharply as the channel is forced into depletion. The energy profiles (U vs. Q_{ch}), obtained by integrating Q_{ch} with respect to bias V_{ox} across the Ta_2O_5 , are plotted in Figures 3 (c) and (d) during the forward and backward sweeps of gate bias. Owing to the accumulation and sudden depletion of the mobile oxygen ions, the energy profiles show inflection points in the regions marked $c \rightarrow d$ and $a \rightarrow b$, leading to $d^2U/dQ_{ch}^2 < 0$ in these regions. The corresponding inverse unit area capacitances, plotted in Figures 3 (e) and (f), show C_{EL} less than zero in these regions, with a magnitude greater than C_{ins} ($\sim 67 \text{ nF/cm}^2$, measured from MIM structures), which also causes the total capacitance $C_{tot}(= C_{ins} + C_{EL})$ to become negative. Following equation (3), this leads to a body factor less than unity. The reason why a sub- 60 mV/dec switching is only present during $a \rightarrow b$ in the backward sweep but not during $c \rightarrow d$ in the forward sweep, is because Q_{ox} remains negative during the transition from $c \rightarrow d$ (see Figure 3 (b)), a polarity which depletes the carriers in the channel. Therefore, the device shows no switching in this region and continues to remain in the off-state. This parallel system of capacitance C_{tot} is stabilised by the capacitance of the ZnO semiconductor, which appears in series with Ta_2O_5 gate insulator, since the required condition for stability $|C_{EL} + C_{ins}| > C_{sc}$ is satisfied (The values of C_{EL} and C_{sc} are listed in Table S2 in the supporting information).

gate bias. Potential energy profiles during (c) forward and (d) backward gate sweeps are indicated by arrows. The corresponding inverse unit area capacitance with respect to sheet charge density in the channel during (e) forward and (f) backward gate sweeps.

The electrical characteristics of an SE- and an FE-FET under steady-state, are compared in Figures 4 (a) and 4 (b) for the forward and backward sweeps of the gate bias. In Figure 4 (a), since the ions in the SE have sufficient time to respond to an infinitesimally small scan rate, the hysteresis observed previously, now vanishes, the build-up of Q_{ox} remains limited only by the balance between drift (responsible for accumulation) and diffusion (responsible for depletion) of ions. The steep-switching also vanishes, since Q_{ox} simultaneously increases or decreases alongside the gate bias under equilibrium and the energy profile reduces to a single energy-well without any inflection point, as shown in the inset of Figure 4 (a). In stark contrast, in an equivalent FE-FET simulated in Figure 4 (b), the existence of a double energy-well profile, as shown in the inset gives rise to hysteresis in transfer characteristics, even if the bias is swept quasi-statically. Moreover, while the SS in the present device becomes greater than 60 mV/dec under quasi-static operation, it continues to remain less than 60 mV/dec in a FE-FET. This distinction that is directly based upon their underlying mechanisms, sets both types of devices apart.

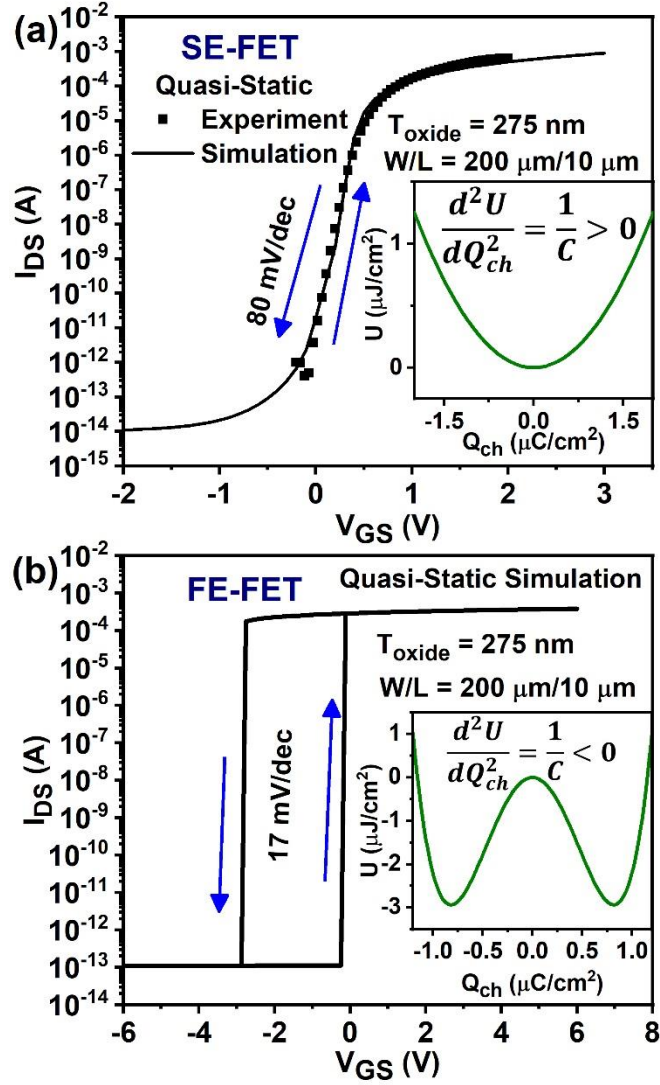


Figure 4. Quasi-static transfer characteristics for SE- and FE- FETs. Comparison of transfer characteristics of an (a) SE-FET and (b) FE-FET both at a scan frequency of $33 \mu\text{Hz}$ where the device characteristics tend towards their corresponding quasi-static behaviour, FE-FET is simulated using $\alpha = -3 \times 10^{11} \text{ cm}/F$, $\beta = 6.8 \times 10^{23} \text{ cm}^5/FC^2$, $\gamma = 0$, and $\rho = 4 \times 10^{11} \Omega \text{ cm}$.

The mechanism of vacancy migration inside Ta_2O_5 is limited to thin films of Ta_2O_5 or TaO_x ($\sim 5 - 20 \text{ nm}$)^{18,32,37-41}, where a migration of ions and vacancies leads to the formation of a vacancy rich conductive filament inside Ta_2O_5 , much smaller than the thickness of our films. Our

measured gate current of the order of a few nanoamperes eliminates the possibility of any filamentary process (cf. inset, Figure 2 (a)). Moreover, the temperature dependence of the transfer characteristics, as presented in Supplementary Figure S2, further supports our claim that the observed phenomena is due to the movements of oxygen ions. According to the point ion model of Mott and Gurney, a rise in the temperature results in a higher mobility of the ions. Therefore, at a higher temperature, the higher mobility of ions contributes to a larger Q_{ox} , which produces an increase in the drain current during the forward bias. This enhancement with respect to a change in gate bias also leads to an earlier depletion of Q_{ox} during the reverse sweep, resulting in a smaller hysteresis.

The distinction in operation of our device is further established via an examination of the dynamic characteristics with frequency. The SS slope during the forward and backward gate bias sweep in the entire frequency range is summarised in Figures 5 (a) and (b). The model of an SE-FET in Figure 5 (a) exhibits $SS < 60 \text{ mV/dec}$ only in the frequency range $\sim 2.2 - 20 \text{ mHz}$ highlighted by the oval, showing good agreement in both forward and backward sweeps with experiment. The value of steep switching during the backward sweep is sensitive to the maximum accumulated Q_{ox} and its subsequent depletion as the gate bias is reduced. As the frequency of gate sweep is increased further, the transfer characteristics of SE-FETs tend towards that of a thin film transistor (TFT) with an ordinary insulator as the gate dielectric at higher frequency. In Supplementary Figure S3, the transfer characteristics of an SE-FET at a sweep frequency of 10 mHz , where movement of ions is significant is compared with that at 21 Hz . The latter, acting as a baseline-FET, highlights the impact of neglecting the motion of ions in the insulator. Moreover, close to steady state the SS is 80 mV/dec , attesting to the excellent quality of the interface. In contrast, the dependence of the SS of a simulated FE-FET shown in 5 (b) reveals

values less than 60 mV/dec for both forward and backward scans up to $\sim 10 \mu\text{Hz}$, where the device tends towards the quasi-static mode with both forward and backward sweep having identical slopes, for $\rho = 3 \times 10^{12} \Omega \text{ cm}$. Beyond this point, the hysteresis between the forward and backward transfer characteristics becomes larger due to the finite delay in the switching of domains as determined by ρ , which leads to an increase/decrease in SS during the forward/backward sweeps respectively. As the frequency of gate sweep increases from 50 to 60 mHz , the response of the domains in the ferroelectric with respect to the applied gate bias become smaller due their incapability to follow the fast-changing gate bias. This results in a decrease in the polarization charge, which directly corresponds to a smaller drain current. Consequently, in this range of sweep frequency, the subthreshold slope of the device in both forward and backward directions shows an increase, due to the smaller changes in the drain current with applied gate bias. At a sweep frequency of 60 mHz or beyond, the domains in the ferroelectric stop responding to the changes in gate bias, leading to constant carrier density in the channel. Thus the drain current no longer shows any switching with gate bias. Although not shown, the hysteresis of the SE-FET becomes zero at very low and high sweep frequencies where the SS for both forward and backward sweeps become identical, whereas the hysteresis in a FE-FET, if not stabilised, can persist even for identical SS in the forward and backward sweeps, as seen in Figure 4 (b).

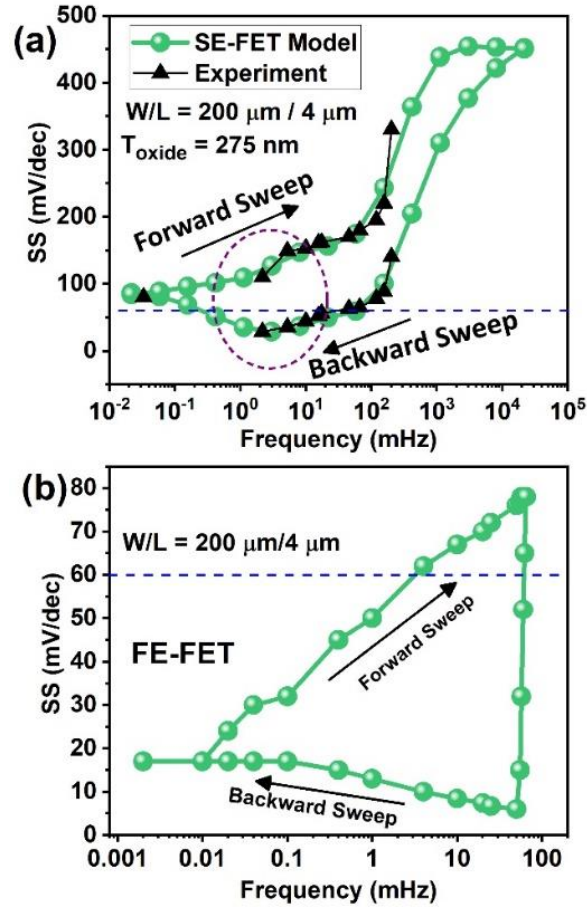


Figure 5. SS vs. frequency of SE- and FE- FETs. (a) Subthreshold swing (SS) of an SE-FET with frequency of scan rate in the forward and backward directions of gate bias. (b) SS versus frequency of a FE-FET (simulated using $\alpha = -3.2 \times 10^{11} \text{ cm}/F$, $\beta = -6.8 \times 10^{23} \text{ cm}^5/FC^2$, $\gamma = 0$, and $\rho = 3 \times 10^{12} \Omega \text{ cm}$) showing a below $60 \text{ mV}/\text{dec}$ of switching at low frequency of operation in both forward and backward sweeps in contrast to the SE-FET.

Finally, Figure 6 (a) shows a comparison of transfer characteristics during the backward scan of a SE-FET obtained from the model and measurement at different oxide thicknesses at a scan frequency of 2.17 mHz . An increased drain to source on-current for the higher oxide thickness

suggests the presence of higher sheet density of oxide ions Q_{ox} due to an increased number of mobile species, as shown in Supplementary Figure S4. The value of n_{ion} and x_D used in the simulation for calibration are listed in Supplementary Table S2, which also summarizes the extracted values of C_{ins} , C_{EL} , C_{SC} , body factor and subthreshold swing in the region of steep switching for the two thicknesses of Ta_2O_5 . The scaling behaviour of an SE-FET is contrary to the scaling laws of FE-FETs of the same thickness, especially in the region of subthreshold switching, illustrated in Figure 6 (b). FE-FETs show a cross-over point in their scaling⁴² with a greater insulator thickness, effectively reducing the electric field and thereby the polarisation due to alignment of dipoles, leading to a smaller density of carriers in the channel.

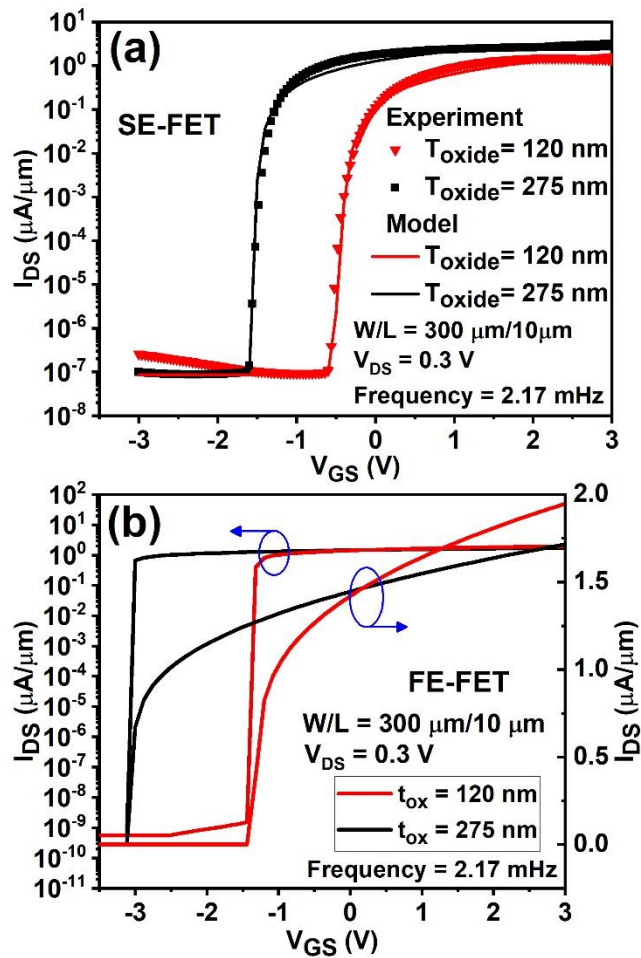


Figure 6. Comparison of the SE-FET and FE-FET transfer characteristics at different gate dielectric thicknesses. (a) Experimental and modelled transfer characteristics in the reverse sweep of SE-FETs with oxide thicknesses of 120 and 275 nm and corresponding simulated behaviour, showing higher maximum on-current of $3.63 \mu A/\mu m$ for the thicker insulator and $1.8 \mu A/\mu m$ for thinner, at a gate-bias of 3 V, while the SS is $28 mV/dec$ and $48 mV/dec$ for both respectively. (b) shows the dependence of the ON current in log and linear scales in a FE-FET which follows a conventional scaling rule, i.e, thicker oxide device revealing lower on-current, while the SS for both the thicknesses is $\sim 16 mV/dec$ (simulated using $\alpha = -3 \times 10^{11} cm/F$, $\beta = 6.8 \times 10^{23} cm^5/FC^2$, $\gamma = 0$, and $\rho = 4 \times 10^{11} \Omega cm$). A cross-over point with gate voltage is observed in the characteristics.

An extrapolation of drain current characteristics and SS characteristics obtained from our simulation model to smaller thicknesses of Ta_2O_5 , as provided in Supplementary Figures S5 (a) and (b), indicates that at 20 nm, hysteresis in the drain current shrinks to $\sim 0.2 V$, while the SS no longer remains smaller than $60 mV/dec$, in the backward sweep.

The presence of hysteresis in SE-FETs aligns well with applications such as biological synapses in neuromorphic applications¹⁹. These devices are ideally suited for logic-in-memory via crossbar arrays rather than conventional CMOS. From a knowledge of the density and mobility of oxygen ions, the presented model can be used to predict device behaviour, i.e. the amount of hysteresis and swing for a particular sweep frequency of gate bias. The model shows that frequency of operation is directly proportional to the mobility of oxygen ions μ_{ion} . For example, an order of magnitude boost in μ_{ion} will increase the scan frequency by an order, to produce electrical characteristics with the same swing. Therefore, by adjusting μ_{ion} , e.g. with temperature, these

devices can be operated at even higher frequency, e.g. $\sim 1\text{ Hz}$, a desirable frequency in neuromorphic applications.

CONCLUSION

The theory and mechanism leading to a new class of negative capacitance FETs is unveiled here using an example of a Ta_2O_5/ZnO FET. It is shown that the field driven motion of ions and vacancies in the gate insulator (Ta_2O_5) leads to an accumulation of charge at the interface of the semiconductor. The dispersion of this charge during the reverse sweep, without any filamentary process, creates a negative differential capacitance, responsible for steep switching as low as 26 mV/dec in the mHz range in these devices via a body factor effectively less than unity. Here we prove irrevocably that the switching behaviour observed in our case, is primarily different from the mechanism arising from a dual energy landscape responsible for the switching in FE-FETs, by scrutinising the relationship of SS with the frequency in the forward and backward directions. Distinct characteristics of SE-FET identified in this work demonstrate a representative class of devices with a solid/liquid electrolyte as gate insulator, whose performance can be tuned via control of the diffusivity of ions. This class of materials therefore opens up unique opportunities for optimisation of device performance via control of interfacial phenomena in semiconductor devices.

ASSOCIATED CONTENT

Supporting Information

The following files are available free of charge.

Derivation of the body factor of the SE-FET; a description of the model of the dynamic transfer characteristics of the SE-FET; Tables listing the parameters of ZnO and Ta_2O_5 used in the model; Measured device characteristics with temperature highlighting the influence of mobility of ions;

Comparison of the simulated transfer characteristics of an SE-FET at two different frequencies highlighting the influence of ionic motion; Variation of the sheet density of the oxide ions at the Ta_2O_5/ZnO interface, with gate bias, for different Ta_2O_5 thickness; Simulated $I_{DS} - V_{GS}$ and SS characteristics at different thicknesses of Ta_2O_5 layer (PDF).

AUTHOR INFORMATION

Corresponding Author

*Email: m.desouza@sheffield.ac.uk

Author Contributions

M.M.S directed this work to explain the SS switching in comparison to FE-FETs including identification of the key factors such as switching speed, oxide scaling. A.K developed the equations and undertook the modelling to demonstrate these effects with respect to experimental data. P.B.P prepared the samples, and characterised the data from measurements, with contributions from X.S. The manuscript was primarily written by MMS and AK. All authors have given approval to the final version of the manuscript.

Conflict of Interest

The authors declare no competing financial interests.

ACKNOWLEDGMENT

We gratefully acknowledge funds from the ENIAC JU project E2SG under grant number 296131.

REFERENCES

- (1) Datta, S. *Quantum Transport : Atom to Transistor*; 2005.
- (2) Ionescu, A. M.; Riel, H. Tunnel Field-Effect Transistors as Energy-Efficient Electronic

- Switches. *Nature* **2011**, *479*, 329–337.
- (3) 2013 ITRS - International Technology Roadmap for Semiconductors.
 - (4) Nikonov, D. E.; Young, I. A. Overview of Beyond-CMOS Devices and a Uniform Methodology for Their Benchmarking. *Proc. IEEE* **2013**, *101*, 2498–2533.
 - (5) Jain, A.; Alam, M. A. Prospects of Hysteresis-Free Abrupt Switching (0 MV/Decade) in Landau Switches. *IEEE Trans. Electron Devices* **2013**, *60*, 4269–4276.
 - (6) Zhirnov, V. V.; Cavin, R. K. Nanoelectronics: Negative Capacitance to the Rescue? *Nat. Nanotechnol.* **2008**, *3*, 77–78.
 - (7) Park, J. H.; Jang, G. S.; Kim, H. Y.; Seok, K. H.; Chae, H. J.; Lee, S. K.; Joo, S. K. Sub-KT/q Subthreshold-Slope Using Negative Capacitance in Low-Temperature Polycrystalline-Silicon Thin-Film Transistor. *Sci. Rep.* **2016**, *6*, 24734.
 - (8) Salahuddin, S.; Datta, S. Use of Negative Capacitance to Provide Voltage Amplification for Low Power Nanoscale Devices. *Nano Lett.* **2008**, *8*, 405–410.
 - (9) Then, H. W.; Dasgupta, S.; Radosavljevic, M.; Chow, L.; Chu-Kung, B.; Dewey, G.; Gardner, S.; Gao, X.; Kavalieros, J.; Mukherjee, N.; *et al.* Experimental Observation and Physics of “Negative” Capacitance and Steeper than 40mV/Decade Subthreshold Swing in Al_{0.83}In_{0.17}N/AlN/GaN MOS-HEMT on SiC Substrate. In *2013 IEEE International Electron Devices Meeting*; IEEE, 2013; p. 28.3.1-28.3.4.
 - (10) Jana, R. K.; Snider, G. L.; Jena, D. On the Possibility of Sub 60 MV/Decade Subthreshold Switching in Piezoelectric Gate Barrier Transistors. *Phys. Status Solidi Curr. Top. Solid State Phys.* **2013**, *10*, 1469–1472.

- (11) Loh, O. Y.; Espinosa, H. D. Nanoelectromechanical Contact Switches. *Nat. Nanotechnol.* **2012**, *7*, 283–295.
- (12) Lee, J. O.; Song, Y.-H.; Kim, M.-W.; Kang, M.-H.; Oh, J.-S.; Yang, H.-H.; Yoon, J.-B. A Sub-1-Volt Nanoelectromechanical Switching Device. *Nat. Nanotechnol.* **2013**, *8*, 36–40.
- (13) Kim, J. H.; Chen, Z. C. Y.; Kwon, S.; Xiang, J. Three-Terminal Nanoelectromechanical Field Effect Transistor with Abrupt Subthreshold Slope. *Nano Lett.* **2014**, *14*, 1687–1691.
- (14) Shukla, N.; Thathachary, A. V; Agrawal, A.; Paik, H.; Aziz, A.; Schlom, D. G.; Gupta, S. K.; Engel-Herbert, R.; Datta, S. A Steep-Slope Transistor Based on Abrupt Electronic Phase Transition. *Nat. Commun.* **2015**, *6*, 7812.
- (15) Song, J.; Woo, J.; Lee, S.; Prakash, A.; Yoo, J.; Moon, K.; Hwang, H. Steep Slope Field-Effect Transistors With Ag/TiO₂-Based Threshold Switching Device. *IEEE Electron Device Lett.* **2016**, *37*, 932–934.
- (16) Menzel, S.; Bottger, U.; Wimmer, M.; Salinga, M. Physics of the Switching Kinetics in Resistive Memories. *Adv. Funct. Mater.* **2015**, *25*, 6306–6325.
- (17) Tappertzhofen, S.; Valov, I.; Tsuruoka, T.; Hasegawa, T.; Waser, R.; Aono, M. Generic Relevance of Counter Charges for Cation-Based Nanoscale Resistive Switching Memories. *ACS Nano* **2013**, *7*, 6396–6402.
- (18) Wedig, A.; Luebben, M.; Cho, D.-Y.; Moors, M.; Skaja, K.; Rana, V.; Hasegawa, T.; Adepalli, K. K.; Yildiz, B.; Waser, R.; *et al.* Nanoscale Cation Motion in TaO_x, HfO_x and TiO_x Memristive Systems. *Nat. Nanotechnol.* **2015**, *11*, 67–74.
- (19) Balakrishna Pillai, P.; De Souza, M. M. Nanoionics-Based Three-Terminal Synaptic Device

- Using Zinc Oxide. *ACS Appl. Mater. Interfaces* **2017**, *9*, 1609–1618.
- (20) Xu, C.; Xiao, Q.; Ma, J.; Jin, Y.; Shao, J.; Fan, Z. High Temperature Annealing Effect on Structure, Optical Property and Laser-Induced Damage Threshold of Ta₂O₅ Films. *Appl. Surf. Sci.* **2008**, *254*, 6554–6559.
- (21) Balakrishna Pillai, P.; Kumar, A.; Song, X.; De Souza, M. M. Diffusion-Controlled Faradaic Charge Storage in High-Performance Solid Electrolyte-Gated Zinc Oxide Thin-Film Transistors. *ACS Appl. Mater. Interfaces* **2018**, *10*, 9782–9791.
- (22) Ye, Z.; Yuan, Y.; Xu, H.; Liu, Y.; Luo, J.; Wong, M. Mechanism and Origin of Hysteresis in Oxide Thin-Film Transistor and Its Application on 3-D Nonvolatile Memory. *IEEE Trans. Electron Devices* **2017**, *64*, 438–446.
- (23) Gallagher, P.; Lee, M.; Petach, T. A.; Stanwyck, S. W.; Williams, J. R.; Watanabe, K.; Taniguchi, T.; Goldhaber-Gordon, D. A High-Mobility Electronic System at an Electrolyte-Gated Oxide Surface. *Nat. Commun.* **2015**, *6*, 6437.
- (24) Yoon, J.; Hong, W. K.; Jo, M.; Jo, G.; Choe, M.; Park, W.; Sohn, J. I.; Nedic, S.; Hwang, H.; Welland, M. E.; *et al.* Nonvolatile Memory Functionality of ZnO Nanowire Transistors Controlled by Mobile Protons. *ACS Nano* **2011**, *5*, 558–564.
- (25) Nasr, B.; Wang, D.; Kruk, R.; Rosner, H.; Hahn, H.; Dasgupta, S. High-Speed, Low-Voltage, and Environmentally Stable Operation of Electrochemically Gated Zinc Oxide Nanowire Field-Effect Transistors. *Adv. Funct. Mater.* **2013**, *23*, 1750–1758.
- (26) Lu, A.; Sun, J.; Jiang, J.; Wan, Q. Low-Voltage Transparent Electric-Double-Layer ZnO-Based Thin-Film Transistors for Portable Transparent Electronics. *Appl. Phys. Lett.* **2010**,

96, 043114.

- (27) Shulman, J.; Xue, Y. Y.; Tsui, S.; Chen, F.; Chu, C. W. General Mechanism for Negative Capacitance Phenomena. *Phys. Rev. B - Condens. Matter Mater. Phys.* **2009**, *80*, 1–6.
- (28) Gommans, H. H. P.; Kemerink, M.; Janssen, R. A. J. Negative Capacitances in Low-Mobility Solids. *Phys. Rev. B* **2005**, *72*, 235204.
- (29) Wang, Y.-F.; Lin, Y.-C.; Wang, I.-T.; Lin, T.-P.; Hou, T.-H. Characterization and Modeling of Nonfilamentary Ta/TaOx/TiO2/Ti Analog Synaptic Device. *Sci. Rep.* **2015**, *5*, 10150.
- (30) Mott, N. F.; Gurney, R. W. *Electronic Processes in Ionic Crystals*; Oxford: Clarendon Press, 1940.
- (31) Kim, S.; Kim, S.-J.; Kim, K. M.; Lee, S. R.; Chang, M.; Cho, E.; Kim, Y.-B.; Kim, C. J.; Chung, U.-I.; Yoo, I.-K. Physical Electro-Thermal Model of Resistive Switching in Bi-Layered Resistance-Change Memory. *Sci. Rep.* **2013**, *3*, 1680.
- (32) Kim, W.; Menzel, S.; Wouters, D. J.; Guo, Y.; Robertson, J.; Roesgen, B.; Waser, R.; Rana, V. Impact of Oxygen Exchange Reaction at the Ohmic Interface in Ta2O5-Based ReRAM Devices. *Nanoscale* **2016**, *8*, 17774–17781.
- (33) Liu, C. M.; Liu, W. L.; Chen, W. J.; Hsieh, S. H.; Tsai, T. K.; Yang, L. C. ITO as a Diffusion Barrier Between Si and Cu. *J. Electrochem. Soc.* **2005**, *152*, G234–G239.
- (34) Lee, S. T.; Gao, Z. Q.; Hung, L. S. Metal Diffusion from Electrodes in Organic Light-Emitting Diodes. *Appl. Phys. Lett.* **1999**, *75*, 1404–1406.
- (35) Schlatmann, A. R.; Floet, D. W.; Hilberer, A.; Garten, F.; Smulders, P. J. M.; Klapwijk, T.

- M.; Hadziioannou, G. Indium Contamination from the Indium-Tin-Oxide Electrode in Polymer Light-Emitting Diodes. *Appl. Phys. Lett.* **1996**, *69*, 1764–1766.
- (36) Bard, A. J.; Faulkner, L. R. *Electrochemical Methods: Fundamentals and Applications*; Wiley, 2001.
- (37) Moors, M.; Adepalli, K. K.; Lu, Q.; Wedig, A.; Bäumer, C.; Skaja, K.; Arndt, B.; Tuller, H. L.; Dittmann, R.; Waser, R.; *et al.* Resistive Switching Mechanisms on TaO_x and SrRuO₃ Thin-Film Surfaces Probed by Scanning Tunneling Microscopy. *ACS Nano* **2016**, *10*, 1481–1492.
- (38) Valov, I.; Linn, E.; Tappertzhofen, S.; Schmelzer, S.; van den Hurk, J.; Lentz, F.; Waser, R. Nanobatteries in Redox-Based Resistive Switches Require Extension of Memristor Theory. *Nat. Commun.* **2013**, *4*, 1771.
- (39) Lübben, M.; Karakolis, P.; Ioannou-Sougleridis, V.; Normand, P.; Dimitrakis, P.; Valov, I. Graphene-Modified Interface Controls Transition from VCM to ECM Switching Modes in Ta/TaO_x Based Memristive Devices. *Adv. Mater.* **2015**, *27*, 6202–6207.
- (40) Siemon, A.; Breuer, T.; Aslam, N.; Ferch, S.; Kim, W.; Van Den Hurk, J.; Rana, V.; Hoffmann-Eifert, S.; Waser, R.; Menzel, S.; *et al.* Realization of Boolean Logic Functionality Using Redox-Based Memristive Devices. *Adv. Funct. Mater.* **2015**, *25*, 6414–6423.
- (41) Skaja, K.; Bäumer, C.; Peters, O.; Menzel, S.; Moors, M.; Du, H.; Bornhöfft, M.; Schmitz, C.; Feyer, V.; Jia, C. L.; *et al.* Avalanche-Discharge-Induced Electrical Forming in Tantalum Oxide-Based Metal-Insulator-Metal Structures. *Adv. Funct. Mater.* **2015**, *25*,

7154–7162.

- (42) Duarte, J. P.; Khandelwal, S.; Khan, A. I.; Sachid, A.; Lin, Y.; Chang, H.; Salahuddin, S.; Hu, C. Compact Models of Negative-Capacitance FinFETs: Lumped and Distributed Charge Models. In *2016 IEEE International Electron Devices Meeting (IEDM)*; IEEE, 2016; Vol. 5, p. 30.5.1-30.5.4.

TABLE OF CONTENTS FIGURE

